

Finite-volume Hamiltonian method for coupled channel interactions in lattice QCD

Jia-Jun Wu,¹ T.-S. H. Lee,¹ A. W. Thomas,^{2,3} and R. D. Young^{2,3}

¹*Physics Division, Argonne National Laboratory, Argonne, Illinois 60439, USA*

²*Special Research Center for the Subatomic Structure of Matter (CSSM),
School of Chemistry and Physics, University of Adelaide Adelaide 5005, Australia*

³*ARC Center of Excellence for Particle Physics at Terascale,
School of Chemistry and Physics, University of Adelaide Adelaide 5005, Australia*

Abstract

Within a multi-channel formulation of $\pi\pi$ scattering, we investigate the use of the finite-volume Hamiltonian approach to relate lattice QCD spectra to scattering observables. The equivalence of the Hamiltonian approach and the coupled-channel extension of the well-known Lüscher formalism is established. Unlike the single channel system, the spectra at a single lattice volume in the coupled channel case do not uniquely determine the scattering parameters. We investigate the use of the Hamiltonian framework as a method to directly fit the lattice spectra and thereby extract the scattering phase shifts and inelasticities. We find that with a modest amount of lattice data, the scattering parameters can be reproduced rather well, with only a minor degree of model dependence.

PACS numbers: 25.20.Lj, 24.85.+p

I. INTRODUCTION

Lattice QCD studies are making tremendous progress in resolving the excitation spectrum of QCD [1–5]. By the nature of the finite-volume and Euclidean time aspects of the lattice formulation, it is impossible to directly simulate scattering processes. The established way to extract of scattering information from lattice simulations is the Lüscher method [6, 7]. For the case of elastic 2-body scattering, Lüscher identified that the energy eigenstates on a finite volume have a one-to-one correspondence with the scattering phase shifts (up to exponentially suppressed corrections associated with quantum fluctuations of the lightest degrees of freedom in the system). The extension of this formalism to incorporate inelastic channels was developed by He, Feng and Liu [8], and is the topic of considerable further investigations [9–18].

Unlike the single channel case, the finite-volume energy eigenstates of a multichannel system no longer exhibit a unique correspondence with the parameters of the S -matrix. For example, in the case of two coupled channels on a given volume, the energy eigenstate is determined by a single condition relating the three asymptotic scattering parameters (i.e. two phase shifts and an inelasticity). Therefore the only way to uniquely identify all three parameters would be to search for coincident energy eigenstates at either different volumes or with different momentum boosts of the system [17]. Alternatively, one requires some form of interpolation which can reproduce the scattering parameters with a limited set of lattice simulation results. In the present work, we extend a recently developed finite-volume Hamiltonian formalism [19] to a coupled-channel system. We establish the equivalence of the coupled-channel Hamiltonian formalism with the extensions of Lüscher’s method. Further, we investigate the inversion problem of extracting the phase shifts and inelasticity from a finite set of pseudo lattice data. We find that all three scattering parameters can be reliably reproduced by directly constraining the parameters of the model to the finite volume spectra. In the energy region constrained by the fits, the extracted phase shifts and inelasticity show only a mild sensitivity to the precise form of the model.

To facilitate the exploration of LQCD spectra, our analysis is based upon a two-channel Hamiltonian formulation which is constructed by fitting the available $\pi\pi$ scattering phase shifts data in the $J^{IP} = 0^{0+}, 1^{1-}$ partial waves. The explicit channels included are $\pi\pi$ and the inelasticity associated with $K\bar{K}$ production.

In section II, we write down a multi-channel formulation for constructing several model Hamiltonians from fitting the $\pi\pi$ scattering data. The model with only the $\pi\pi$ channel is used in section III to recall the finite-box Hamiltonian method developed in Ref. [19] and to examine the correspondence with Luscher’s formula. In section IV, we use the model with $\pi\pi$ and $K\bar{K}$ channels to show that the finite-box Hamiltonian approach is equivalent to the approach based on the two-channel Lüscher’s method developed in Ref. [8]. In section IV, we compare the LQCD efforts needed to apply the finite-box Hamiltonian approach and the approach based on Lüscher’s method. Our predictions of the spectra for testing LQCD results for $\pi\pi$ scattering in the $J^{IP} = 0^{0+}, 1^{1-}$ partial waves are presented in section V. In section VI, we give a summary and discuss possible future developments.

II. MODEL HAMILTONIAN FOR $\pi\pi$ SCATTERING

The Hamiltonian with only vertex interactions, such as $\Delta \leftrightarrow \pi N$ considered in Ref.[19], is the simplest example within the general multi-channel formulation, inspired by the cloudy

bag model [20, 21] and developed in Ref. [22] for investigating the nucleon resonances [23] and meson resonances [24]. For investigating the finite-box Hamiltonian approach in this work, it is useful to recall the formulation of Refs. [22, 24] in order to write down a general Hamiltonian for $\pi\pi$ scattering.

Following Refs. [22, 24], we assume that $\pi\pi$ scattering can be described by vertex interactions and two-body potentials. In the rest frame, the model Hamiltonian of a meson-meson system takes the following *energy-independent* form

$$H = H_0 + H_I. \quad (1)$$

The non-interacting part is

$$H_0 = \sum_{i=1,n} |\sigma_i\rangle m_i^0 \langle \sigma_i| + \sum_{\alpha} |\alpha\rangle [\sqrt{m_{\alpha_1}^2 + \vec{k}_{\alpha_1}^2} + \sqrt{m_{\alpha_2}^2 + \vec{k}_{\alpha_2}^2}] \langle \alpha|, \quad (2)$$

where σ_i is the i -th bare particle with mass m_i^0 , $\alpha = \pi\pi, K\bar{K}, \pi\eta, \dots$ denotes the channels included, and m_{α_i} and \vec{k}_{α_i} are the mass and the momentum operator of the i -th particle in the channel α , respectively.

The interaction Hamiltonian is

$$H_I = g + v, \quad (3)$$

where g is a vertex interaction describing the decays of the bare particles into two-particle channels α, β, \dots

$$g = \sum_{\alpha} \sum_{i=1,n} \{ |\alpha\rangle g_{i,\alpha}^\dagger \langle i| + |i\rangle g_{i,\alpha} \langle \alpha| \} \quad (4)$$

and the direct two-to-two particle interaction is defined by

$$v = \sum_{\alpha,\beta} |\alpha\rangle v_{\alpha,\beta} \langle \beta|. \quad (5)$$

In each partial wave, the two particle scattering is then defined by the following coupled-channel equations

$$t_{\alpha,\beta}(k, k'; E) = V_{\alpha,\beta}(k, k') + \sum_{\gamma} \int_0^\infty k''^2 dk'' V_{\alpha,\gamma}(k, k'') \frac{1}{E - E_{\gamma_1}(k'') - E_{\gamma_2}(k'') + i\epsilon} t_{\gamma,\beta}(k'', k'; E) \quad (6)$$

where $E_{\gamma i} = \sqrt{k''^2 + m_{\gamma i}^2}$, and the coupled-channel potentials are

$$V_{\alpha,\beta}(k, k') = \sum_{i=1,n} g_{i,\alpha}^*(k) \frac{1}{E - m_i^0} g_{i,\alpha}(k') + v_{\alpha,\beta}(k, k') \quad (7)$$

with

$$g_{i,\alpha}(k) = \langle i|g|\alpha(k)\rangle \quad (8)$$

$$v_{\alpha,\beta}(k, k') = \langle \alpha(k)|v|\beta(k')\rangle \quad (9)$$

We choose the normalization, $\langle \vec{k} | \vec{k}' \rangle = \delta(\vec{k} - \vec{k}')$, such that the S-matrix in each partial-wave is related to the T-matrix by

$$S_{\alpha,\beta}(E) = 1 + 2iT_{\alpha,\beta}(k_{0\alpha}, k_{0\beta}; E) \quad (10)$$

with

$$T_{\alpha,\beta}(k_{0\alpha}, k_{0\beta}; E) = -\rho_\alpha^{1/2}(k_{0\alpha}) t_{\alpha,\beta}(k_{0\alpha}, k_{0\beta}; E) \rho_\beta^{1/2}(k_{0\beta}) \quad (11)$$

where $k_{0\alpha}$ is the on-shell momentum for the channel α and the density of states is

$$\rho_\alpha(k_{0\alpha}) = \pi \frac{k_{0\alpha} E_{\alpha 1}(k_{0\alpha}) E_{\alpha 2}(k_{0\alpha})}{E_{\alpha 1}(k_{0\alpha}) + E_{\alpha 2}(k_{0\alpha})} \quad (12)$$

In the following sections, we construct (1) one-bare state and one-channel ($1b - 1c$) models, (2) one-bare state and two-channels ($1b - 2c$) models, and also (3) two-bare states and two-channels ($2b - 2c$) models.

III. ONE BARE STATE AND ONE-CHANNEL

In this section, we consider a model which has one bare state (σ) and one-channel ($\pi\pi$) to describe the isoscalar s -wave $\pi\pi$ scattering phase shifts up to the energy below the $K\bar{K}$ threshold. The formulae for constructing this model, called $1b - 1c$ model, can be obtained from taking $n = 1$ and $\alpha = \beta = \gamma = \pi\pi$ in section II.

A. Model parameters

For simplicity, we parametrize the matrix elements of the interactions in Eqs.(4) and (5) as

$$\begin{aligned} \langle \sigma | g | k \rangle &= g_{\sigma,\pi\pi}(k) \\ &= \frac{g_{\pi\pi}}{\sqrt{\pi}} \frac{1}{(1 + (c_{\pi\pi} \times k)^2)}, \end{aligned} \quad (13)$$

$$\begin{aligned} \langle k | v | k' \rangle &= v_{\pi\pi,\pi\pi}(k, k') \\ &= \frac{G_{\pi\pi,\pi\pi}}{m_\pi^2} \times \frac{1}{(1 + (d_{\pi\pi} \times k)^2)^2} \times \frac{1}{(1 + (d_{\pi\pi} \times k')^2)^2}, \end{aligned} \quad (14)$$

where k and k' are the three momenta of π in the center of mass system. By fitting the $\pi\pi$ phase shifts, the parameters, m_σ , $g_{\pi\pi}$, $c_{\pi\pi}$, $G_{\pi\pi,\pi\pi}$ and $d_{\pi\pi}$, of the model can be determined and are listed in the column “1b-1c” in Table I. The calculated phase shifts are compared with the data in Fig. 1. The model gives a reasonable description of the data and is sufficient for exploring the systematics of the finite-volume Hamiltonian method.

B. Finite-volume Hamiltonian

The finite-volume Hamiltonian method provides direct access to the multi-particle energy eigenstates in a periodic volume characterised by side length L . The quantised three

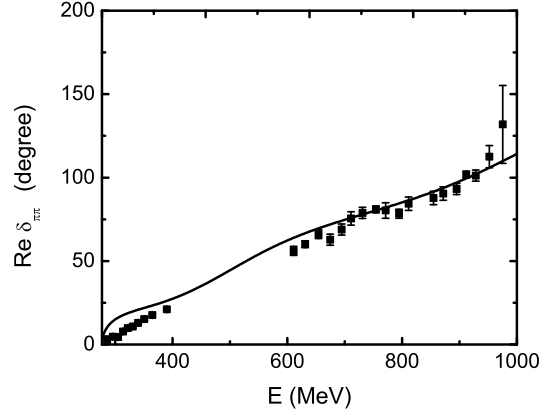


FIG. 1: The phase shifts of $\pi\pi$ scattering from the Model 1b-1c (cf. Table I) are compared with the data.

TABLE I: The parameters for the 1 bare state and 1 channel ($1b - 1c$) model, and the 1 bare state and 2 channel ($1b - 2c$) model

	1b-1c	1b-2c
$m_\sigma(\text{MeV})$	700.	700.00
$g_{\sigma\pi\pi}$	1.6380	2.0000
$c_{\sigma\pi\pi}(\text{fm})$	1.0200	0.6722
$G_{\pi\pi, \pi\pi}$	0.5560	2.4998
$d_{\pi\pi}(\text{fm})$	0.5140	0.2440
$g_{\sigma K\bar{K}}$	-	0.6451
$c_{\sigma K\bar{K}}(\text{fm})$	-	1.0398
$G_{K\bar{K}, K\bar{K}}$	-	0.0200
$d_{K\bar{K}}(\text{fm})$	-	0.1000
$G_{\pi\pi, K\bar{K}}$	-	0.3500

momenta of the π meson must be $k_n = \sqrt{n} \frac{2\pi}{L}$ for integers $n = 0, 1, 2, \dots$. For a given choice of N momenta $(k_0, k_1, \dots, k_{N-1})$, solving the Schrodinger equation $H|\Psi_E\rangle = E|\Psi_E\rangle$ in the finite box is equivalent to finding the solutions of the following matrix equations

$$\det([H_0]_{N+1} + [H_I]_{N+1} - E[I]_{N+1}) = 0 \quad (15)$$

where \det is taking the determinant of a matrix, $[I]_{N+1}$ is an $(N+1) \times (N+1)$ unit matrix, and the non-interaction Hamiltonian H_0 , defined by Eq.(2), is represented by the following $(N+1) \times (N+1)$ matrix

$$[H_0]_N = \begin{pmatrix} m_\sigma & 0 & 0 & \dots \\ 0 & 2\sqrt{k_0^2 + m_\pi^2} & 0 & \dots \\ 0 & 0 & 2\sqrt{k_1^2 + m_\pi^2} & \dots \\ \vdots & \vdots & \vdots & \ddots \end{pmatrix}, \quad (16)$$

With the forms of the interactions g and v in Eqs.(4)-(5), the $N \times N$ matrix representing the interaction Hamiltonian H_I can be written as

$$[H_I]_N = \begin{pmatrix} 0 & g_{\pi\pi}^{fin}(k_0) & g_{\pi\pi}^{fin}(k_1) & \cdots \\ g_{\pi\pi}^{fin}(k_0) & v_{\pi\pi,\pi\pi}^{fin}(k_0, k_0) & v_{\pi\pi,\pi\pi}^{fin}(k_0, k_1) & \cdots \\ g_{\pi\pi}^{fin}(k_1) & v_{\pi\pi,\pi\pi}^{fin}(k_1, k_0) & v_{\pi\pi,\pi\pi}^{fin}(k_1, k_1) & \cdots \\ \vdots & \vdots & \vdots & \ddots \end{pmatrix}. \quad (17)$$

The corresponding finite-volume matrix elements are given by

$$g_{\pi\pi}^{fin}(k_n) = \sqrt{\frac{C_3(n)}{4\pi}} \left(\frac{2\pi}{L}\right)^{3/2} g_{\sigma,\pi\pi}(k_n), \quad (18)$$

$$v_{\pi\pi,\pi\pi}^{fin}(k_{n_1}, k_{n_2}) = \sqrt{\frac{C_3(n_1)}{4\pi}} \sqrt{\frac{C_3(n_2)}{4\pi}} \left(\frac{2\pi}{L}\right)^3 v_{\pi\pi,\pi\pi}(k_{n_1}, k_{n_2}), \quad (19)$$

where $g_{\pi\pi}(k_n)$ and $v_{\pi\pi,\pi\pi}(k_{n_1}, k_{n_2})$ are defined in Eqs.(13)-(14), and $C_3(n)$ represents the number of ways of summing the squares of three integers to equal n . As explained in Ref.[19], the factor $\sqrt{\frac{C_3(n)}{4\pi}} \left(\frac{2\pi}{L}\right)^{3/2}$ follows from the quantization conditions in a finite box with size L .

The solution of Eq.(15) is a spectrum which depends on the choice of the box size L and N . Obviously, the acceptable solution must converge as N increases. To get high accuracy results for examining Lüscher's formula, we find that $N = 600$ is sufficient for a range of L in our calculations. The predicted spectra for each L can be read from the solid curves shown in Fig. 2. The dashed curves indicate the free-particle spectra (ie. in the absence of interactions).

C. Phase shift extraction

As reported in Ref. [19], the Hamiltonian and Lüscher methods predict almost identical finite volume spectra. Here we demonstrate this by using the Lüscher formalism to extract the phase shift from the finite volume spectra. The appropriate formulae are summarised in Appendix A. By sampling the spectrum at a discrete set of hypothetical volumes, shown in Fig. 2, we invert to obtain the phase shifts shown in Fig. 3. Here we see an excellent reproduction of the model phase shifts. A couple of points show a small deviation from the exact curve. These correspond to the smallest volume, $L = 5$ fm, where the exponentially suppressed corrections are beginning to be relevant.

In comparison with realistic lattice calculations, we note that the smooth reproduction of the phase shift would require significant resources in terms of the number of volumes sampled. Such a dense extraction of the phase shift is more easily made possible by studying the spectra in moving frames, such as Ref. [5, 25–29]. The extension of the Hamiltonian formalism to such boosted systems will be investigated in future work.

With the equivalence with the Lüscher technique demonstrated, we now turn to the extension to multi-channel scattering.

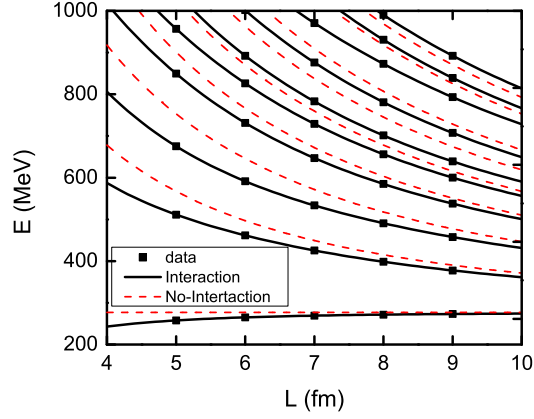


FIG. 2: The spectrum of $\pi\pi$ states in the $1b - 1c$ model. The black curves are calculated by using the finite-volume Hamiltonian approach. The boxes denote discrete points on these curves which are used in the phase extraction shown in Fig. 3.

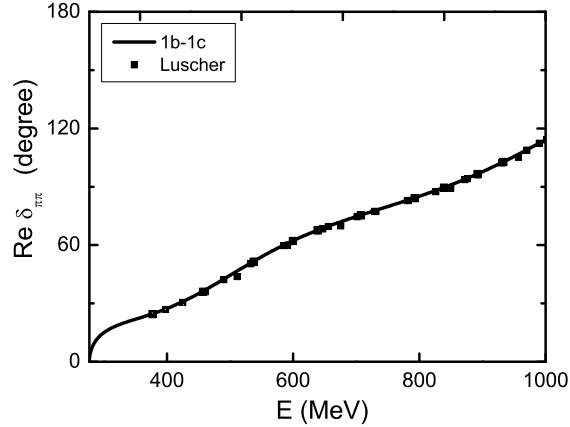


FIG. 3: The black curve is generated from directly solving scattering equations Eqs.(6)-(7), and the solid squares are calculated from using the Lüscher's method by using the spectrum appearing in Fig. 2.

IV. ONE BARE STATE AND TWO-CHANNELS

A. Model parameters

To describe $\pi\pi$ scattering above the $K\bar{K}$ threshold, we construct a model with one bare state and two-channels. The formula for such a model can be obtained from Section II by setting $n = 1$ for a bare particle σ and $\alpha, \beta, \gamma = \pi\pi, K\bar{K}$. Similar to the $1b - 1c$ model of section III, the matrix elements of the interactions defined in Eqs.(4) and (5) are

parameterized as

$$\begin{aligned}\langle\sigma|g|\alpha(k)\rangle &= g_{\sigma,\alpha}(k) \\ &= \frac{g_{\sigma,\alpha}}{\sqrt{\pi}} \frac{1}{(1 + (c_\alpha \times k)^2)},\end{aligned}\tag{20}$$

$$\begin{aligned}\langle\alpha(k)|v|\beta(k')\rangle &= v_{\alpha,\beta}(k, k') \\ &= \frac{G_{\alpha,\beta}}{m_\pi^2} \times \frac{1}{(1 + (d_\alpha \times k)^2)^2} \times \frac{1}{(1 + (d_\beta \times k')^2)^2},\end{aligned}\tag{21}$$

with k and k' are the three momenta of π or K in the center mass system. There are ten parameters: m_σ , $g_{\pi\pi}$, $c_{\pi\pi}$, $g_{K\bar{K}}$, $c_{K\bar{K}}$, $G_{\pi\pi, \pi\pi}$, $G_{\pi\pi, K\bar{K}}$, $G_{K\bar{K}, K\bar{K}}$, $d_{\pi\pi}$ and $d_{K\bar{K}}$. By fitting the data of $\pi\pi$ phase shift δ and inelasticity η , the model parameters can be determined and are listed in the second column of Table I. The calculated phase shifts are compared with the data in Figs. 4–6. As in the single channel case, the agreement is sufficiently good for our exploration of the finite volume Hamiltonian method.

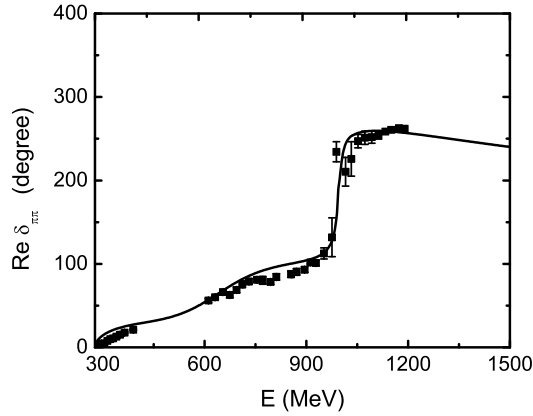


FIG. 4: The phase shift $\delta_{\pi\pi}$ for $\pi\pi$ scattering from the $1b - 2c$ model are compared with the data.

B. Finite-volume Hamiltonian method

To calculate the spectrum for the $1b - 2c$ model constructed in the previous subsection, we follow the procedures given in Section III B to extend the matrix representation of the Hamiltonian to include the elements associated with the additional $K\bar{K}$ channel for each mesh points of the chosen N momenta $k_n = \sqrt{n} \frac{2\pi}{L}$ for $n = 0, 1, 2 \dots (N-1)$. This leads to the following $(2N+1) \times (2N+1)$ matrix equations

$$\det([H_0]_{2N+1} + [H_I]_{2N+1} - E[I]_{2N+1}) = 0\tag{22}$$

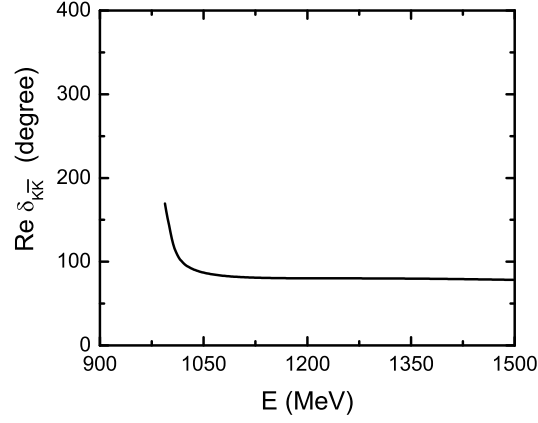


FIG. 5: The phase shift $\delta_{K\bar{K}}$ of $K\bar{K}$ scattering calculated in the $1b - 2c$ model.

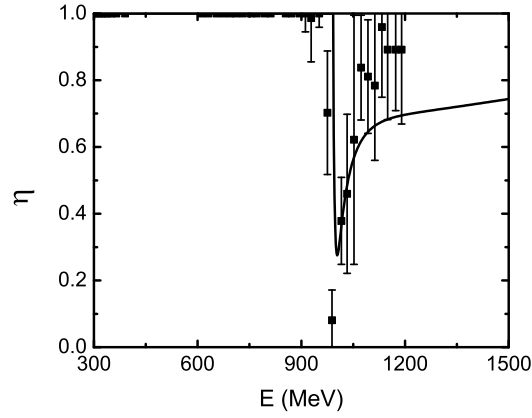


FIG. 6: The inelasticity η in the $1b - 2c$ model compared with the data.

where $[I]_{2N+1}$ is an $(2N + 1) \times (2N + 1)$ unit matrix, and

$$[H_0]_{2N+1} = \begin{pmatrix} m_0 & 0 & 0 & 0 & 0 & \cdots \\ 0 & 2\sqrt{k_0^2 + m_\pi^2} & 0 & 0 & 0 & \cdots \\ 0 & 0 & 2\sqrt{k_0^2 + m_K^2} & 0 & 0 & \cdots \\ 0 & 0 & 0 & 2\sqrt{k_1^2 + m_\pi^2} & 0 & \cdots \\ 0 & 0 & 0 & 0 & 2\sqrt{k_1^2 + m_K^2} & \cdots \\ \vdots & \vdots & \vdots & \vdots & \vdots & \ddots \end{pmatrix}$$

The $(2N + 1) \times (2N + 1)$ matrix for the interaction Hamiltonian is

$$[H_I]_{2N+1} = \begin{pmatrix} 0 & g_{\pi\pi}^{fin}(k_0) & g_{K\bar{K}}^{fin}(k_0) & g_{\pi\pi}^{fin}(k_1) & g_{K\bar{K}}^{fin}(k_1) & \cdots \\ g_{\pi\pi}^{fin}(k_0) & v_{\pi\pi,\pi\pi}^{fin}(k_0, k_0) & v_{\pi\pi,K\bar{K}}^{fin}(k_0, k_0) & v_{\pi\pi,\pi\pi}^{fin}(k_0, k_1) & v_{\pi\pi,K\bar{K}}^{fin}(k_0, k_1) & \cdots \\ g_{K\bar{K}}^{fin}(k_0) & v_{K\bar{K},\pi\pi}^{fin}(k_0, k_0) & v_{K\bar{K},K\bar{K}}^{fin}(k_0, k_0) & v_{K\bar{K},\pi\pi}^{fin}(k_0, k_1) & v_{K\bar{K},K\bar{K}}^{fin}(k_0, k_1) & \cdots \\ g_{\pi\pi}^{fin}(k_1) & v_{\pi\pi,\pi\pi}^{fin}(k_1, k_0) & v_{\pi\pi,K\bar{K}}^{fin}(k_1, k_0) & v_{\pi\pi,\pi\pi}^{fin}(k_1, k_1) & v_{\pi\pi,K\bar{K}}^{fin}(k_1, k_1) & \cdots \\ g_{K\bar{K}}^{fin}(k_1) & v_{K\bar{K},\pi\pi}^{fin}(k_1, k_0) & v_{K\bar{K},K\bar{K}}^{fin}(k_1, k_0) & v_{K\bar{K},\pi\pi}^{fin}(k_1, k_1) & v_{K\bar{K},K\bar{K}}^{fin}(k_1, k_1) & \cdots \\ \vdots & \vdots & \vdots & \vdots & \vdots & \ddots \end{pmatrix},$$

with

$$g_{\alpha}^{fin}(k_n) = \sqrt{\frac{C_3(n)}{4\pi}} \left(\frac{2\pi}{L}\right)^{3/2} g_{\sigma,\alpha}(k_n), \quad (23)$$

$$v_{\alpha,\beta}^{fin}(k_{n_i}, k_{n_j}) = \sqrt{\frac{C_3(n_i)}{4\pi}} \sqrt{\frac{C_3(n_j)}{4\pi}} \left(\frac{2\pi}{L}\right)^3 v_{\alpha,\beta}(k_{n_i}, k_{n_j}), \quad (24)$$

where $g_{\sigma,\alpha}(k_n)$ and $v_{\alpha,\beta}(k_{n_i}, k_{n_j})$ are defined in Eqs. (20) and (21). In this way, we can generate the spectrum from the Hamiltonian in a finite box with a given size L by solving Eq. (22). The computed spectrum is shown as a function of the volume in Fig. 7.

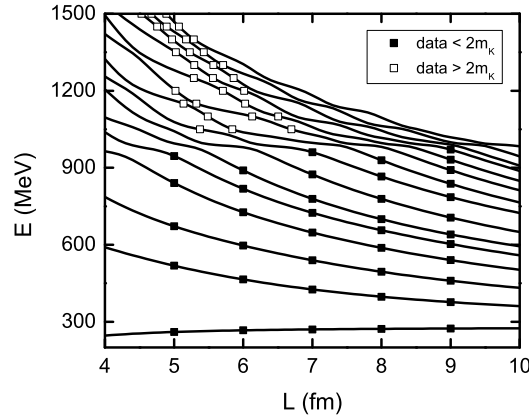


FIG. 7: The black curves show the energy spectra generated by using the finite-box Hamiltonian approach within the the $1b - 2c$ model. The solid and open squares are selected solutions below and above the inelastic threshold, respectively. These solutions have been inverted through the extended Lüscher formalism to determine the phase shifts and inelasticities, see Fig. 9.

C. Multi-channel spectra

Our first task here is to establish the equivalence of the Hamiltonian spectrum with that of the multi-channel generalisation of Lüscher. The relevant formulae for the coupled-channel

system are summarised in Appendix A 2. For the present case, the eigenvalue spectrum (above the inelastic threshold) is defined by the solutions to the following equation

$$\begin{aligned} & \cos[\phi(q_{\pi\pi}) + \phi(q_{K\bar{K}}) - \delta_{\pi\pi}(E) - \delta_{K\bar{K}}(E)] \\ & - \eta(E) \cos[\phi(q_{\pi\pi}) - \phi(q_{K\bar{K}}) - \delta_{\pi\pi}(E) + \delta_{K\bar{K}}(E)] = 0. \end{aligned} \quad (25)$$

The phase ϕ characterises the lattice geometry as defined by Eq. (A3). Knowledge of the energy-dependence of the phase shifts and inelasticity allows one to determine the spectrum for a given value of L . The eigenvalue equation is solved for E , where the dimensionless momenta, $q_\alpha = k_\alpha L/(2\pi)$, corresponding to the on-shell momentum k_α in channel α (see Eq. (A2)).

Using the model phase shifts and inelasticities, the Lüscher-style formalism allows one to uniquely determine the finite volume spectrum. For this model, the solutions of Eq. (25) (in the inelastic region) are shown in Fig. 8. The predicted spectra within the two approaches are in excellent agreement.

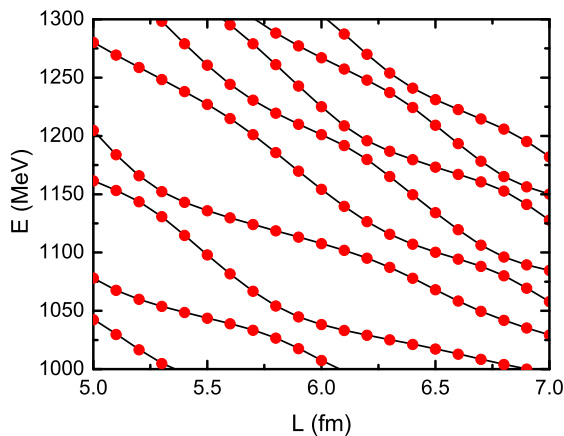


FIG. 8: The solid dots represent the finite volume spectrum as determined by the extended Lüscher formalism; computed directly from the model phase shifts and inelasticities. These are in excellent agreement with the spectra computed with the Hamiltonian approach, as shown by the continuous curves.

Of relevance to lattice QCD simulations is the desire to obtain $\delta_{\pi\pi}$, $\delta_{K\bar{K}}$ and η from the spectra determined in numerical simulations. Using Eq. (A8), the isolation of all three scattering parameters at any given E would require eigenstates at this energy for three different box sizes. Such solutions are indicated by the white squares in Fig. 7. An impractical ensemble of lattice volumes would be required to carry out such a study. As an example, at $E = 1200$ MeV, with box sizes $L = 5.022, 5.708, 6.014$ fm, the model spectrum can be inverted through Eq. (A8) to determine

$$\delta_{\pi\pi} = 256.5^\circ, \quad \delta_{K\bar{K}} = 79.84^\circ, \quad \eta = 0.6980. \quad (26)$$

We note the relative phase between $\delta_{\pi\pi}$ and $\delta_{K\bar{K}}$ is only determined up to integer multiples of π — an ambiguity that has been elaborated on in Ref. [30]. Up to the determination of this phase, we note excellent agreement with the underlying model scattering,

$$\delta_{\pi\pi} = 256.6^\circ, \quad \delta_{K\bar{K}} = 80.18^\circ, \quad \eta = 0.6965. \quad (27)$$

The extraction of $\delta_{\pi\pi}$ in this way, for a range of energies, is shown by the white squares in Fig. 9. In the following Section we explore the inversion from finite volume spectra using a discrete ensemble of lattice volumes, as would be the case in practice.

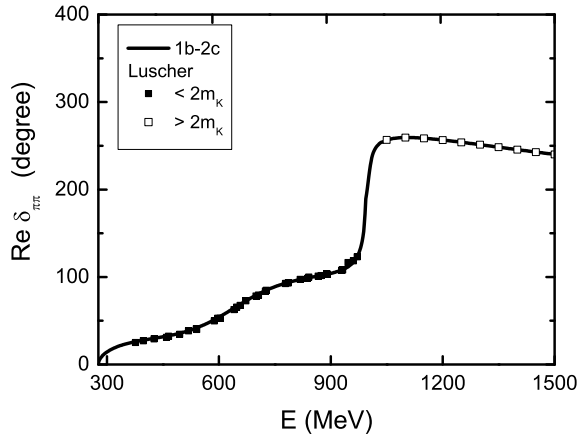


FIG. 9: The black curve denotes the model $\pi\pi$ phase shift. The solid and open squares denote the inversion of the solutions shown in Fig. 7 below and above the inelastic thresholds. Below the inelastic threshold, each solution uniquely determines the phase shift. Above the inelastic threshold, the unique solution requires the impractical determination of three identical energy levels at different L . In this region, $\delta_{K\bar{K}}$ and η (Figs. 5 and 6) are equally-well described by this inversion.

V. APPLICATIONS TO LQCD

We investigate the procedure for using the Hamiltonian approach to predict the scattering observables from the spectrum generated from LQCD. We will compare our approach with the approach based on Lüscher’s formula. For this illustrative purpose, it is sufficient to use the $1b-1c$ and $1b-2c$ models described in sections III and IV to generate the spectra which will be referred to as the “LQCD data”. The phase shifts at each energy of these spectra are of course known, as shown as the solid curves in Figs. 1 and 4–6.

Our procedure is to use a Hamiltonian to fit a given choice of the spectrum data by solving the eigenvalue problem defined by Eqs.(15)-(19) for the one-channel case and Eqs.(22)-(24) for the two-channel case. We then use the determined Hamiltonian to calculate the phase shifts by using the scattering equations Eqs.(6)-(7) in infinite space.

To proceed, we need to choose the forms of the interactions in Eqs. (1)–(5) of the phenomenological Hamiltonian. For simplicity, we consider the Hamiltonian which has either one bare state and one-channel or one bare state and two-channels. These Hamiltonians are similar to the $1b-1c$ and $1b-2c$ models constructed in sections III and IV, but they can have a different parametrization of the vertex interaction $g_{\sigma,\alpha}$ and $v_{\alpha,\beta}$. We consider three forms:

- A:

$$g(k)_{\sigma,\alpha} = \frac{g_\alpha}{\sqrt{\pi}} \frac{1}{(1 + (c_\alpha \times k)^2)}, \quad (28)$$

$$v_{\alpha,\beta}(k, k') = \frac{G_{\alpha,\beta}}{m_\pi^2} \times \frac{1}{(1 + (d_\alpha \times k)^2)^2} \times \frac{1}{(1 + (d_\beta \times k')^2)^2}, \quad (29)$$

- B:

$$g(k)_{\sigma,\alpha} = \frac{g_\alpha}{\sqrt{\pi}} \frac{1}{(1 + (c_\alpha \times k)^2)^2}, \quad (30)$$

$$v_{\alpha,\beta}(k, k') = \frac{G_{\alpha,\beta}}{m_\pi^2} \times \frac{1}{(1 + (d_\alpha \times k)^2)^4} \times \frac{1}{(1 + (d_\beta \times k')^2)^4}, \quad (31)$$

- C:

$$g(k)_{\sigma,\alpha} = \frac{g_\alpha}{\sqrt{\pi}} e^{-(c_\alpha \times k)^2}, \quad (32)$$

$$v_{\alpha,\beta}(k, k') = \frac{G_{\alpha,\beta}}{m_\pi^2} e^{-(d_\alpha \times k)^2} e^{-(d_\beta \times k')^2}, \quad (33)$$

Note that the parametrization *A* is the same as those of models *1b* – *1c* and *1b* – *2c*, as described above.

A. Fit for one-channel

We first consider the one-channel case. The spectrum data are generated from model *1b* – *1c* constructed in section III. In the left side of Fig. 10, we show 8 data points generated by solving the eigenvalue equation, Eq. (15), for $L = 5, 6$ fm. To see whether the fit depends sensitively on the form of the Hamiltonian, we assign a very small (1 MeV) error for each energy level in the spectrum. We find that these 8 spectrum data points can be fitted by using the parametrization *B*, or *C*, as shown in the left side of Fig.10. The $\pi\pi$ phase shifts calculated from two new Hamiltonians using the scattering equations Eqs. (6)–(7) in infinite space are compared with the data (solid squares) in the right side of Fig. 10. They agree very well in the energy region $E \lesssim 0.9$ GeV, where the spectrum data are fitted. At higher energies, the calculated phase shifts from *B* and *C* deviate from each other and also from the *1b* – *1c* model. Note that both the black solid curves (*A*) and data (solid squares) are from the *1b* – *1c* model and thus they agree with each other completely.

The results presented above suggest that the finite-box Hamiltonian approach is valid in the energy region where the spectrum data are fitted, since the predicted scattering phase shifts are independent of the form of the Hamiltonian and agree with the phase shifts corresponding the fitted spectrum data. To further examine this, we generate 16 data points up to 1.2 GeV and repeat the fitting process. The generated data are the black squares in the left side of Fig.11. The predicted phase shifts agree with the data in the $E < 1.2$ GeV region where the spectrum data are fitted. Above 1.2 GeV they deviate from the *1b* – *1c* model, similar to what we observed in Fig.10.

With the results shown in Figs. 10–11 and the Fig. 2 on Lüscher’s method in section III, we conclude that the finite-volume Hamiltonian approach gives a comparable reproduction

of the phase shifts as compared to Lüscher's method. However, for the one-channel case the finite-volume Hamiltonian method has no distinct advantage over Lüscher's method, since the required LQCD efforts are not so different.

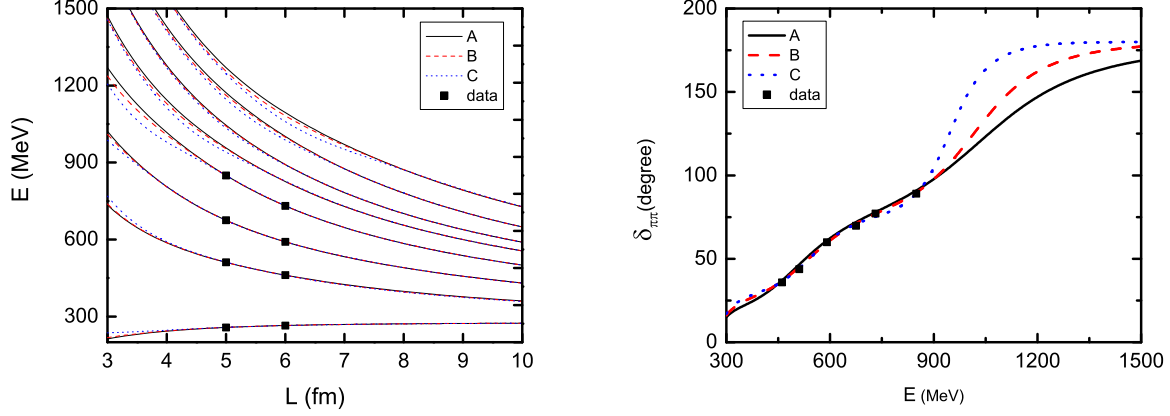


FIG. 10: Left: the spectrum data generated from $1b - 1c$ model. Right: the phase shifts calculated from the one-channels model with parametrization A ($1b - 1c$ model) and B and C specified in Eqs.(28)-(33) are compared with the data (from $1b - 2c$ model).

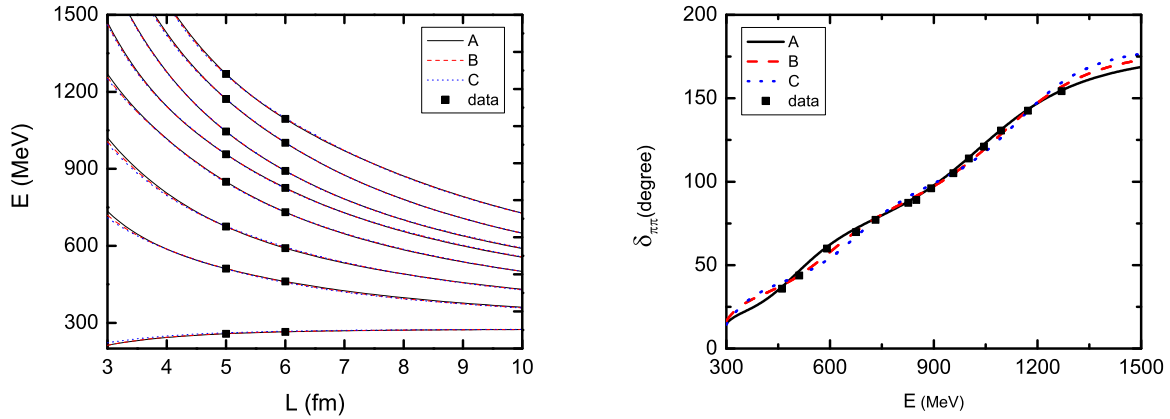


FIG. 11: Left: the spectrum data generated from $1b - 1c$ model. Right: the phase shifts calculated from the one-channels model with the parametrization A ($1b - 1c$ model), B and C specified in Eqs.(28)-(33) are compared with the data (from $1b - 1c$ model).

B. Fit for two-channels

Here we explore the finite-volume Hamiltonian method for the coupled-channels system. We generate 16 and 24 spectrum data points from the $1b - 2c$ model constructed in section

IV.A by solving eigenvalue problem defined by Eqs.(22)-(24) for $L = 5, 6$ fm. As shown in the left top panel of Figs. 12 and 13, these spectrum data can be fit by a Hamiltonian with the parametrization B or C of the interaction Hamiltonian specified in Eqs. (30)–(33). As in the one-channel case, we assign a 1 MeV error for each spectrum data point in these fits. We see in Figs. 12–13 that the phase shifts $\delta_{\pi\pi}$ and $\delta_{K\bar{K}}$ and inelasticity η calculated from the determined Hamiltonians agree well with data (from model $1b - 2c$) in the energy region where the spectrum data are fitted. Similar to the one-channel case, the predicted phase shifts deviate from each other outside the energy range of the fitted spectrum data. We thus conclude that the finite-volume Hamiltonian offers a method to directly extract the scattering parameters from numerical simulation. Furthermore, the

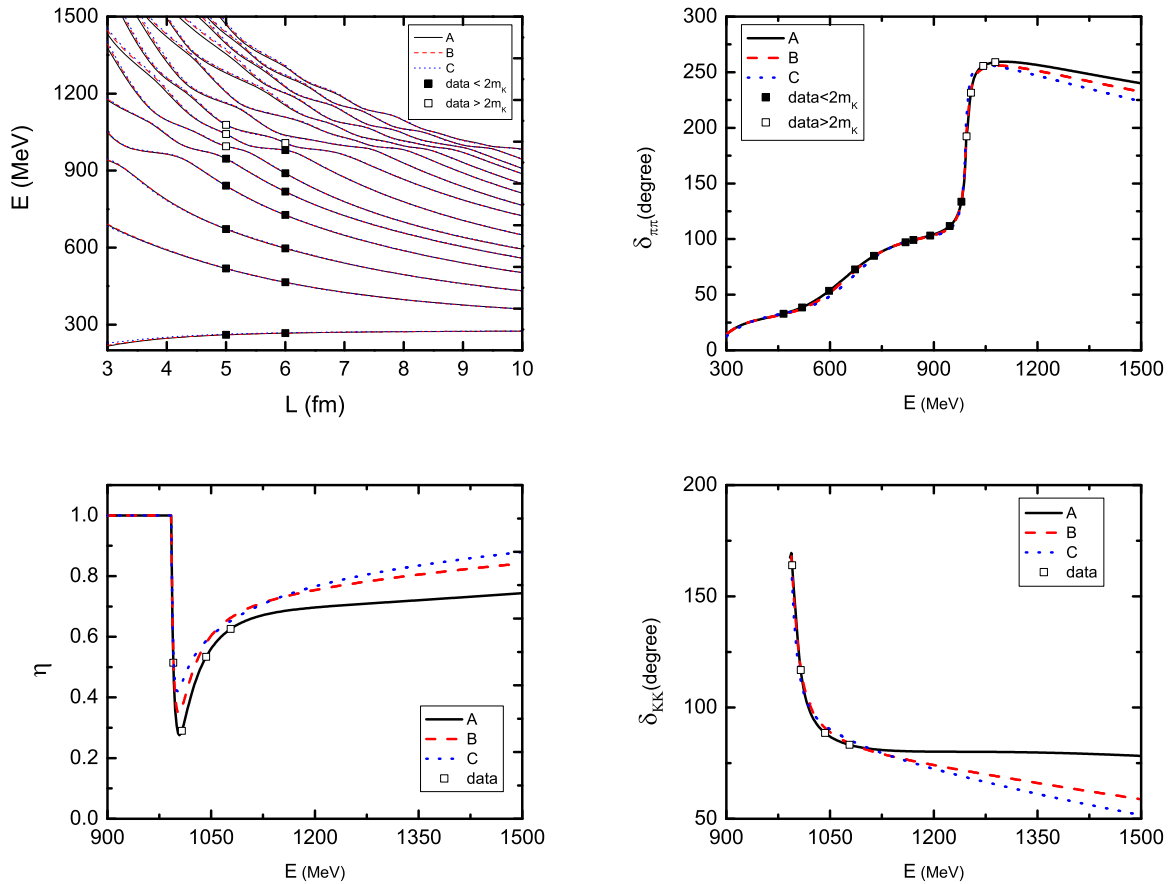


FIG. 12: Left: the spectrum data generated from $1b - 2c$ model. Right: the phase shifts calculated from the two-channels model with the parametrization A ($1b - 2c$ model), B and C specified in Eqs.(28)-(33) are compared with the data (from $1b - 2c$ model).

method is largely independent of the form of the Hamiltonian. One should caution that the resulting Hamiltonian can only be reliably used to predict the scattering observables in the energy region where the lattice spectra are fit — as also seen in the single-channel case.

Here we point out an important difference with the approach using the two-channel Lüscher's formula. As we discussed in section IV, the two-channel Lüscher formula, Eq. (25), needs three spectrum data points at the same energy to calculate two phase shifts and

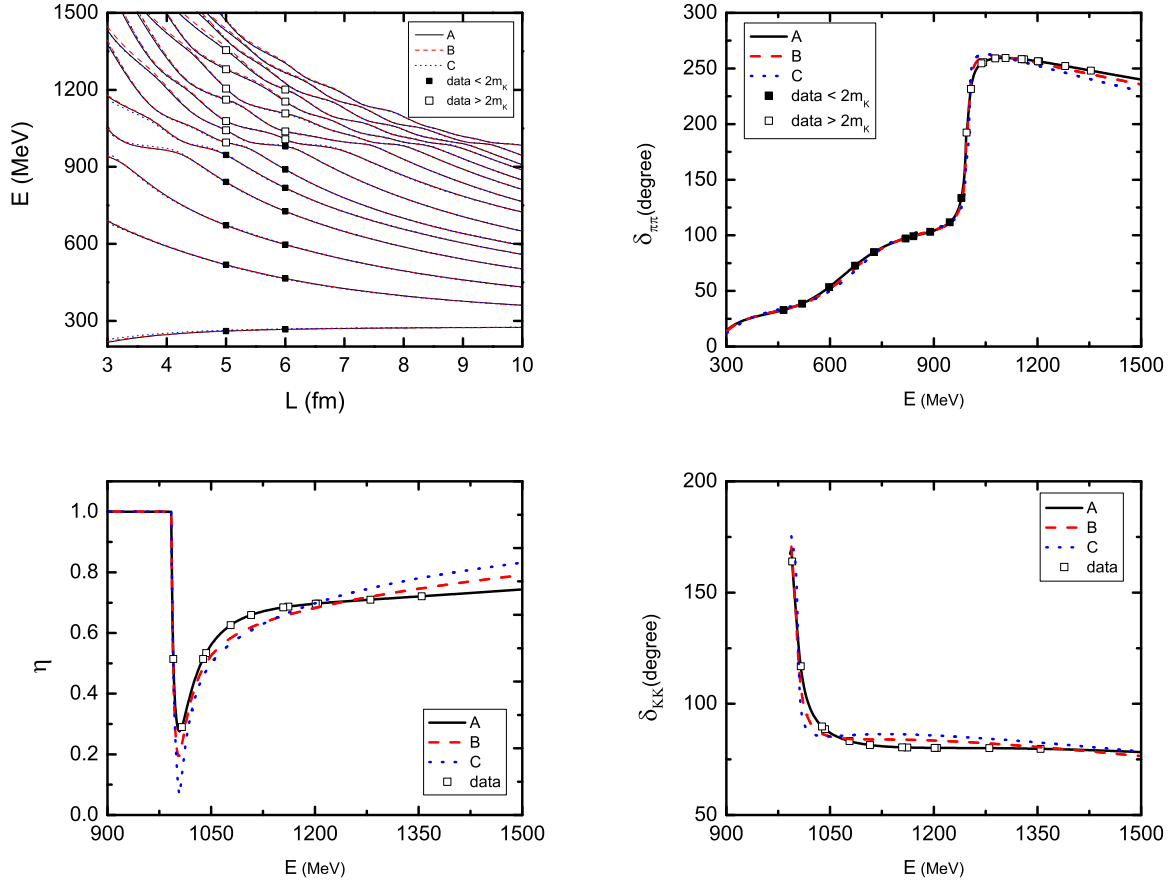


FIG. 13: Left: the spectrum data generated from $1b - 2c$ model. Right: the phase shifts calculated from the one-channels model with the parametrization A ($1b - 2c$ model), B and C specified in Eqs.(28)-(33) are compared with the data (from $1b - 2c$ model).

inelasticity. Thus the spectrum data (open squares) in the left top panel of Figs. 12 and 13 are not sufficient to apply the Lüscher's method. One thus requires many more calculations to get a spectrum like the open squares shown in Fig.9 in section IV. For a given E , we need to get results for three values of L , which can be chosen only after some searches, since we don't know the spectrum for each L before the calculation is finished. Alternatively, the finite-box Hamiltonian method offers a method to interpolate the lattice spectra with a minimal set of volumes. Further, the quality of the extraction will naturally improve more simulation results.

Finally, regarding the relative phase ambiguity mentioned above [30], in the present context of the Hamiltonian formulation, the finite volume spectra cannot fix the relative sign of the resonance coupling to different channels, Eq. (20), nor the sign of the off-diagonal terms in the direct interaction, Eq. (21). Again, these signs only act to constrain the relative phase between $\delta_{\pi\pi}$ and δ_{KK} but do not influence the energy dependence or the isolation of the resonance pole position.

VI. SPECTRA FROM $\pi\pi$ DATA

As a final investigation for the present study, we comment on the possibility of lattice QCD providing the necessary knowledge to improve on phenomenological scattering parameterisations.

Within the Hamiltonian formulation given in section II, the $\pi\pi$ scattering phase shifts $\delta_{\pi\pi}$ and inelasticity η up to 2 GeV have been fit [24] using a model which has two bare states and includes the $\pi\pi$ and $K\bar{K}$ channels. Its interaction Hamiltonian only has the vertex interaction g defined in Eq. (4). This model (which we will refer to as NKLS) also reproduces well the resonance pole positions listed by the Particle Data Group [31]. We explore a further two models, B and C , which further incorporate the two-body interaction v defined in Eq. (5) with the form Eq. (29). These two solutions give equally good fits to the data of $\delta_{\pi\pi}$ and inelasticity η , and the resonance pole positions. The three models for both S-wave and P-wave scattering are shown in Figs. 14 and 15, with model parameters listed in Table II. Note that the parametrization of the matrix elements of the interactions of NKLS model are the same as Model A specified in Eq.(28) and (29) except that the parametrization for the p-wave vertex interaction in the $J^{IP} = 1^{1-}$ partial wave is

$$\begin{aligned} \langle k | g_{\sigma,i} \rangle &= g_{\sigma,i}(k) \\ &= \frac{g_i}{\sqrt{m_\pi}} \left(\frac{1}{(1 + (c_{\pi\pi} \times k)^2)} \right)^{\frac{3}{2}} \frac{k}{m_\pi}, \end{aligned} \quad (34)$$

As there are no data to constrain the $K\bar{K}$ scattering phase shifts, this observable displays the largest variation among the model solutions — see the right panel of Figs. 14 and 15. We can now explore the sensitivity to this variation in the predicted finite volume spectra. These predicted spectra are shown in Fig. 16. While the spectra are in broad agreement between the models, there are noticeable differences among the volumes considered. In particular, on the 4 fm box some energy levels see a variation of up to 50 MeV between the different model solutions. In principle, lattice QCD spectra of this order of precision could act to further constrain this phenomenological model. One should of course caution that, in principle, there could be further inelastic channels appearing in the lattice calculation — such as 4 pions.

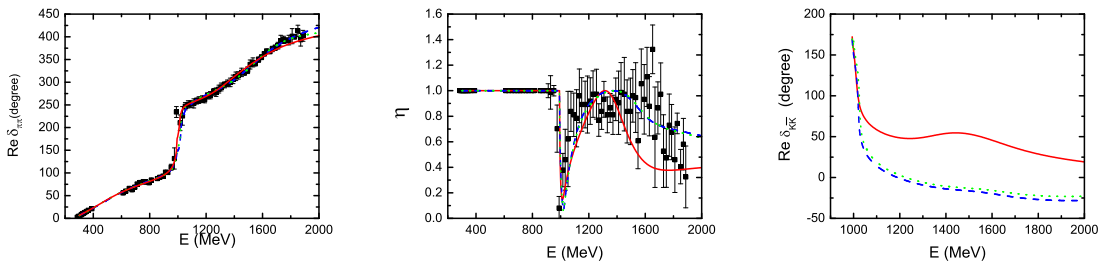


FIG. 14: The phase shifts $\delta_{\pi\pi}$ and $\delta_{K\bar{K}}$, and inelasticity η of s-wave $\pi\pi$ scattering in the $J^{IP} = 1^{0+}$ partial wave. The solid squares are the experiment data. The red solid, blue dashed and green dotted lines are from the NKLS model, Model B, and Model C, respectively.

TABLE II: The parameters of the Hamiltonians from fitting the phase shift data of $\pi\pi$ scattering in s-wave $J^{IP} = 0^{0+}$ and p-wave $J^{IP} = 1^{1-}$ partial waves.

Parameter	S-wave			P-wave		
	NKLS	B	C	NKLS	B	C
$m_{\sigma_1}(\text{MeV})$	1220.0	1094.28	1300.00	891.54	900.000	999.950
$g_{\sigma_1\pi\pi}$	-0.63474	-0.97085	-0.51274	-0.20583	-0.15561	-0.11669
$c_{\sigma_1\pi\pi}(\text{fm})$	0.44658	0.50923	0.33070	0.49998	0.41213	0.31296
$g_{\sigma_1 K\bar{K}}$	0.00605	1.64234	0.07659	0.10607	0.01010	0.00128
$c_{\sigma_1 K\bar{K}}(\text{fm})$	0.10012	2.29463	0.17073	0.42241	0.17333	0.04512
$m_{\sigma_2}(\text{MeV})$	2400.0	1907.63	2318.94	1840.0	1657.66	1903.56
$g_{\sigma_2\pi\pi}$	0.49518	0.49178	1.43296	0.01453	0.01852	0.00517
$c_{\sigma_2\pi\pi}(\text{fm})$	0.20645	0.31107	0.35299	0.10000	0.15068	0.06607
$g_{\sigma_2 K\bar{K}}$	-1.17880	-1.53414	-2.50030	0.16674	2.42851	0.10514
$c_{\sigma_2 K\bar{K}}(\text{fm})$	0.50000	1.06150	0.79294	0.49993	1.71022	0.30817
$G_{\pi\pi, \pi\pi}$	—	0.10000	0.10000	—	-0.01718	0.00024
$G_{\pi\pi, K\bar{K}}$	—	-0.00045	-0.07138	—	-0.11589	-0.04689
$G_{K\bar{K}, K\bar{K}}$	—	-0.00016	0.09992	—	0.34790	0.02819
$d_{\pi\pi}(\text{fm})$	—	0.27088	0.18337	—	0.42441	0.26895
$d_{K\bar{K}}(\text{fm})$	—	0.00551	0.18402	—	0.41520	0.12503
χ^2	305	205	215	189	119	119
Pole(GeV)	$0.43 - 0.27i$	$0.43 - 0.32i$	$0.43 - 0.26i$	$0.77 - 0.081i$	$0.77 - 0.075i$	$0.77 - 0.076i$
	$1.0 - 0.010i$	$1.0 - 0.014i$	$1.0 - 0.008i$	$1.61 - 0.11i$	$1.63 - 0.075i$	$1.65 - 0.083i$
	$1.35 - 0.17i$	$1.51 - 0.22i$	$1.52 - 0.20i$	—	—	—

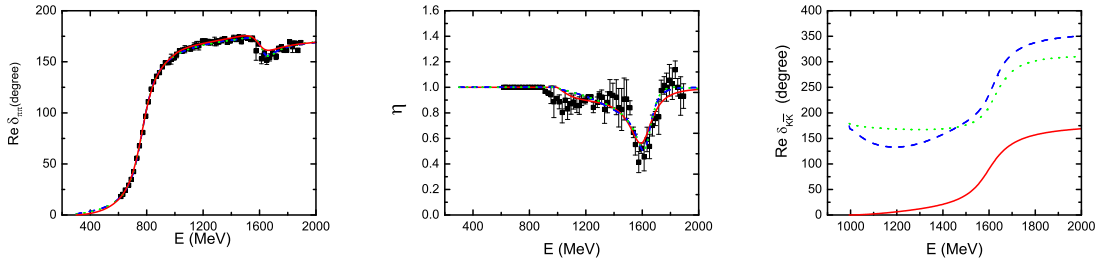


FIG. 15: The phase shifts $\delta_{\pi\pi}$ and $\delta_{K\bar{K}}$, and inelasticity η of p-wave $\pi\pi$ scattering in the $J^{IP} = 1^{1-}$ partial wave. The solid squares are the experiment data. The red solid, blue dashed and green dotted lines are from the NKLS model, Model B, and Model C, respectively.

VII. SUMMARY

We have investigated the finite-volume Hamiltonian method developed in Ref. [19] within several models for $\pi\pi$ scattering. We have demonstrated the equivalence of the finite volume spectra with the Lüscher formalism for both a single channel and also the corresponding generalisation to a coupled-channel system.

We then investigated the practical inversion problem for lattice QCD, with the aim to

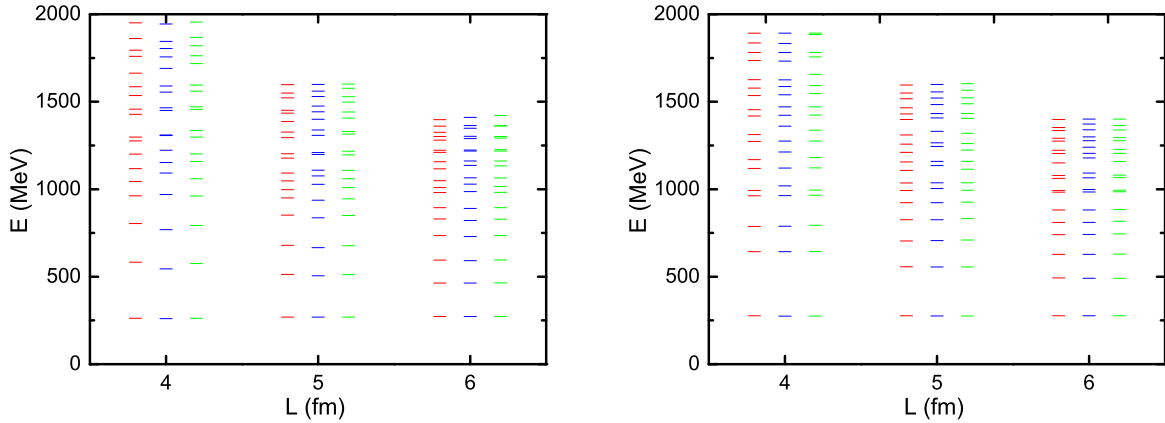


FIG. 16: Spectra for $J^{IP} = 0^{0+}$ (left) and $J^{IP} = 1^{1-}$ (right) partial waves from Models NKLS, Model B and Model C. The spectra have been displaced for clarity.

determine the physical scattering parameters from the finite-volume spectra. In the single-channel system, there is essentially no difference between the Hamiltonian approach and the Lüscher formulation. On the other hand, beyond the inelastic threshold, the finite-volume Hamiltonian offers a much more tractable approach to extract the S-matrix parameters from the finite-volume spectra. We expect this to be further enhanced by the generalisation to moving frames, and this will be investigated in future studies.

Based on phenomenological fits to experimental $\pi\pi$ scattering, we have presented the predicted spectra that one could anticipate seeing in lattice simulations at the physical pion mass. Here we have demonstrated that sufficient precision from lattice QCD simulations would offer the potential to improve the knowledge of these phenomenological models. This is particularly significant for channels that are not directly observable in experiment.

Our investigations are based on a rather phenomenological form of the Hamiltonian. Thus the constructed Hamiltonian from fitting lattice QCD spectrum can not be used reliably to predict scattering observables beyond the energy region where the spectra are fit. One potential improvement in this general framework would be to consider more realistic forms of the Hamiltonian, such as those derived from chiral Lagrangians. This would largely act to improve the near-threshold behaviour of the interactions, however is beyond the scope of the present work.

VIII. ACKNOWLEDGMENT

This work is supported by the U.S. Department of Energy, Office of Nuclear Physics Division, under Contract No. DE-AC02-06CH11357. This research used resources of the National Energy Research Scientific Computing Center, which is supported by the Office of Science of the U.S. Department of Energy under Contract No. DE-AC02-05CH11231, and resources provided on "Fusion", 320-node computing cluster operated by the Laboratory Computing Resource Center at Argonne National Laboratory. This work was also supported by the University of Adelaide and the Australian Research Council through the ARC Centre of Excellence for Particle Physics at the Terascale and grants FL0992247 (AWT),

Appendix A: Lüscher summary

1. Single channel

For comparison with Lüscher’s method, we summarise the formulae relevant to a purely s-wave interaction, as considered in this manuscript. It relates each energy eigenvalues E of the finite box with size L to the scattering phase shift δ at energy E by the following equations:

$$\delta(k) = -\phi(q) + n\pi \quad (\text{A1})$$

with the on-shell momenta given by

$$k = \sqrt{E^2/4 - m_\pi^2}, \quad (\text{A2})$$

and the geometric phase ϕ defined by

$$\tan \phi(q) = -\frac{q\pi^{3/2}}{\mathcal{Z}_{00}(1; q^2)}, \quad (\text{A3})$$

expressed in terms of the lattice momenta

$$q = \frac{kL}{2\pi}. \quad (\text{A4})$$

The generalized zeta function is defined by

$$\mathcal{Z}_{00}(1; q^2) = \frac{1}{\sqrt{4\pi}} \sum_{\vec{n} \in \mathbb{Z}^3} (\vec{n}^2 - q^2)^{-1}, \quad (\text{A5})$$

defined with an appropriate regularisation of the divergent sum (see eg. [7] for discussion). Numerically, a convenient representation for the evaluation of the regularised form is given by

$$\mathcal{Z}_{00}(1; q^2) = \frac{1}{\sqrt{4\pi}} \left(-\frac{1}{q^2} - 8.91363292 + 16.53231596q^2 + \sum_{\vec{n} \in \mathbb{Z}^3, \vec{n} \neq 0} \frac{q^4}{\vec{n}^4(\vec{n}^2 - q^2)} \right). \quad (\text{A6})$$

2. Coupled channel

At energies above the $K\bar{K}$ threshold, we need Lüscher’s method for two open channels, as developed in Ref.[8]. For the considered $\pi\pi$ and $K\bar{K}$ channels, the S -matrix is defined by

$$S = \begin{pmatrix} \eta e^{2i\delta_{\pi\pi}} & i\sqrt{1-\eta^2} e^{i(\delta_{\pi\pi} + \delta_{K\bar{K}})} \\ i\sqrt{1-\eta^2} e^{i(\delta_{\pi\pi} + \delta_{K\bar{K}})} & \eta e^{2i\delta_{K\bar{K}}} \end{pmatrix}, \quad (\text{A7})$$

where the phase shifts $\delta_{\pi\pi}$ and $\delta_{K\bar{K}}$ and inelasticity η at each E are related to the box size L by the following relation

$$\begin{aligned} & \cos[\phi(q_{\pi\pi}) + \phi(q_{K\bar{K}}) - \delta_{\pi\pi}(E) - \delta_{K\bar{K}}(E)] \\ & - \eta(E) \cos[\phi(q_{\pi\pi}) - \phi(q_{K\bar{K}}) - \delta_{\pi\pi}(E) + \delta_{K\bar{K}}(E)] = 0. \end{aligned} \quad (\text{A8})$$

where $\phi(q_\alpha)$ is defined as Eq. (A3), and

$$q_\alpha = \frac{k_\alpha(E)L}{2\pi}. \quad (\text{A9})$$

-
- [1] J. J. Dudek, R. G. Edwards, B. Joo, M. J. Peardon, D. G. Richards and C. E. Thomas, Phys. Rev. D **83**, 111502 (2011) [arXiv:1102.4299 [hep-lat]].
 - [2] R. G. Edwards, J. J. Dudek, D. G. Richards and S. J. Wallace, Phys. Rev. D **84**, 074508 (2011) [arXiv:1104.5152 [hep-ph]].
 - [3] B. J. Menadue, W. Kamleh, D. B. Leinweber and M. S. Mahbub, Phys. Rev. Lett. **108**, 112001 (2012) [arXiv:1109.6716 [hep-lat]].
 - [4] M. S. Mahbub *et al.* [CSSM Lattice Collaboration], Phys. Rev. D **87**, 011501 (2013) [arXiv:1209.0240 [hep-lat]].
 - [5] J. J. Dudek, R. G. Edwards and C. E. Thomas, Phys. Rev. D **87**, no. 3, 034505 (2013) [arXiv:1212.0830 [hep-ph]].
 - [6] M. Luscher, Commun. Math. Phys. **105**, 153 (1986).
 - [7] M. Luscher, Nucl. Phys. B **354**, 531 (1991).
 - [8] S. He, X. Feng and C. Liu, JHEP **0507**, 011 (2005) [hep-lat/0504019].
 - [9] M. Lage, U. -G. Meissner and A. Rusetsky, Phys. Lett. B **681**, 439 (2009) [arXiv:0905.0069 [hep-lat]].
 - [10] V. Bernard, M. Lage, U. -G. Meissner and A. Rusetsky, JHEP **1101**, 019 (2011) [arXiv:1010.6018 [hep-lat]].
 - [11] A. Martinez Torres, L. R. Dai, C. Koren, D. Jido and E. Oset, Phys. Rev. D **85**, 014027 (2012) [arXiv:1109.0396 [hep-lat]].
 - [12] M. Doring and U. G. Meissner, JHEP **1201**, 009 (2012) [arXiv:1111.0616 [hep-lat]].
 - [13] M. T. Hansen and S. R. Sharpe, Phys. Rev. D **86**, 016007 (2012) [arXiv:1204.0826 [hep-lat]].
 - [14] R. A. Briceno and Z. Davoudi, Phys. Rev. D **88**, 094507 (2013) [arXiv:1204.1110 [hep-lat]].
 - [15] M. Doring, U. G. Meissner, E. Oset and A. Rusetsky, Eur. Phys. J. A **48**, 114 (2012) [arXiv:1205.4838 [hep-lat]].
 - [16] N. Li and C. Liu, Phys. Rev. D **87**, 014502 (2013) [arXiv:1209.2201 [hep-lat]].
 - [17] P. Guo, J. Dudek, R. Edwards and A. P. Szczepaniak, Phys. Rev. D **88**, 014501 (2013) [arXiv:1211.0929 [hep-lat]].
 - [18] R. A. Briceno, Z. Davoudi, T. Luu and M. J. Savage, Phys. Rev. D **88**, 114507 (2013) [arXiv:1309.3556 [hep-lat]].
 - [19] J. M. M. Hall, A. C.-P. Hsu, D. B. Leinweber, A. W. Thomas and R. D. Young, Phys. Rev. D **87**, 094510 (2013) [arXiv:1303.4157 [hep-lat]].
 - [20] S. Theberge, A. W. Thomas and G. A. Miller, Phys. Rev. D **22**, 2838 (1980) [Erratum-ibid. D **23**, 2106 (1981)].

- [21] A. W. Thomas, Adv. Nucl. Phys. **13**, 1 (1984).
- [22] A. Matsuyama, T. Sato and T. -S. H. Lee, Phys. Rept. **439**, 193 (2007) [nucl-th/0608051].
- [23] H. Kamano, S. X. Nakamura, T. -S. H. Lee and T. Sato, Phys. Rev. C **88**, 035209 (2013) [arXiv:1305.4351 [nucl-th]]; and other references therein.
- [24] H. Kamano, S. X. Nakamura, T. S. H. Lee and T. Sato, Phys. Rev. D **84**, 114019 (2011) [arXiv:1106.4523 [hep-ph]].
- [25] K. Rummukainen and S. A. Gottlieb, Nucl. Phys. B **450**, 397 (1995) [hep-lat/9503028].
- [26] C. h. Kim, C. T. Sachrajda and S. R. Sharpe, Nucl. Phys. B **727**, 218 (2005) [hep-lat/0507006].
- [27] Z. Fu, Phys. Rev. D **85**, 014506 (2012) [arXiv:1110.0319 [hep-lat]].
- [28] L. Leskovec and S. Prelovsek, Phys. Rev. D **85**, 114507 (2012) [arXiv:1202.2145 [hep-lat]].
- [29] M. Gockeler, R. Horsley, M. Lage, U. -G. Meissner, P. E. L. Rakow, A. Rusetsky, G. Schierholz and J. M. Zanotti, Phys. Rev. D **86**, 094513 (2012) [arXiv:1206.4141 [hep-lat]].
- [30] E. Berkowitz, T. D. Cohen and P. Jefferson, arXiv:1211.2261 [hep-lat].
- [31] J. Beringer *et al.* [Particle Data Group Collaboration], Phys. Rev. D **86**, 010001 (2012).